Three-Dimensional Structure of N^5-Carboxyaminoimidazole Ribonucleotide Synthetase: A Member of the ATP Grasp Protein Superfamily[†,‡]

James B. Thoden,[§] T. Joseph Kappock,[||] JoAnne Stubbe,*[,||] and Hazel M. Holden*[,§]

Department of Biochemistry, University of Wisconsin−Madison, 1710 University Avenue, Madison, Wisconsin 53705, and Departments of Chemistry and Biology, Massachusetts Institute of Technology, Cambridge, Massachusetts 02139

Received July 13, 1999; Revised Manuscript Received August 27, 1999

ABSTRACT: *Escherichia coli* PurK, a dimeric N^5-carboxyaminoimidazole ribonucleotide (N^5-CAIR) synthetase, catalyzes the conversion of 5-aminoimidazole ribonucleotide (AIR), ATP, and bicarbonate to N^5-CAIR, ADP, and P_i. Crystallization of both a sulfate-liganded and the MgADP-liganded *E. coli* PurK has resulted in structures at 2.1 and 2.5 Å resolution, respectively. PurK belongs to the ATP grasp superfamily of C−N ligase enzymes. Each subunit of PurK is composed of three domains (A, B, and C). The B domain contains a flexible, glycine-rich loop (B loop, T_{123}−G_{130}) that is disordered in the sulfate−PurK structure and becomes ordered in the MgADP−PurK structure. MgADP is wedged between the B and C domains, as with all members of the ATP grasp superfamily. Other enzymes in this superfamily contain a conserved Ω loop proposed to interact with the B loop, define the specificity of their nonnucleotide substrate, and protect the acyl phosphate intermediate formed from this substrate. PurK contains a minimal Ω loop without conserved residues. In the reaction catalyzed by PurK, carboxyphosphate is the putative acyl phosphate intermediate. The sulfate of the sulfate ion-liganded PurK interacts electrostatically with Arg 242 and the backbone amide group of Asn 245, components of the J loop of the C domain. This sulfate may reveal the location of the carboxyphosphate binding site. Conserved residues within the C-terminus of the C domain define a pocket that is proposed to bind AIR in collaboration with an N-terminal strand loop helix motif in the A domain (P loop, G_8−L_{12}). The P loop is proposed to bind the phosphate of AIR on the basis of similar binding sites observed in PurN and PurE and proposed in PurD and PurT, four other enzymes in the purine pathway.

In most textbooks the de novo biosynthetic pathway for the production of purines involves 10 enzymatic activities and results in the conversion of phosphoribosyl pyrophosphate to inosine monophosphate (*1*). The sixth step in this pathway is usually represented as a bicarbonate or CO_2-dependent conversion of 5-aminoimidazole ribonucleotide (AIR)[1] to 4-carboxy-5-aminoimidazole ribonucleotide (CAIR), catalyzed by AIR carboxylase. This representation of the pathway has been validated in higher eukaryotes with CO_2 supplying the additional carbon (*2*).

Scheme 1

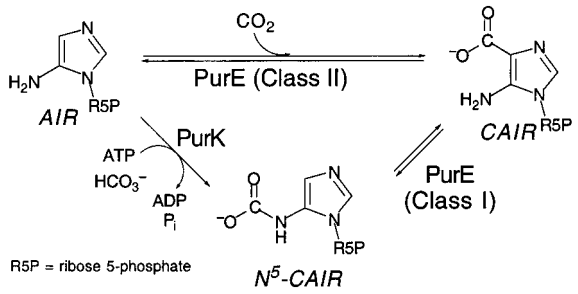

In most prokaryotes, plants, and yeast, however, the conversion of AIR to CAIR requires two gene products: PurK and PurE. PurK has been shown to catalyze the conversion of AIR, ATP, and bicarbonate to N^5-carboxyaminoimidazole ribonucleotide (N^5-CAIR), ADP, and P_i (*3*, *4*). PurE catalyzes the interconversion of N^5-CAIR and CAIR (Scheme 1) (*4*, *5*). The instability of N^5-CAIR, with a $t_{1/2}$ of 15 s at pH 7.5 and 25 °C, delayed its identification and consequently the identification of PurK as an N^5-CAIR synthetase and PurE as an unusual mutase (*4*, *5*). Thus in *E. coli*, yeast, and plants the purine pathway is composed of 11 catalytic activities.

The structures of PurK and PurE are of interest for many reasons. First, channeling, direct transfer by transient protein−

[†] This research was supported in part by grants from the NIH (DK47814 to H.M.H. and GM32191 to J.S.) and the NSF (BIR-9317398). T.J.K. was supported by NIH training grant CA09112.

[‡] X-ray coordinates have been deposited in the Brookhaven Protein Data Bank (1b6r, sulfate complex; 1b6s, MgADP complex) and will be released upon publication.

* To whom correspondence should be addressed: phone (617) 253-1841; fax (617) 258-7247; e-mail stubbe@mit.edu.

[||] University of Wisconsin−Madison.

[§] Massachusetts Institute of Technology.

[1] Abbreviations: N^5-CAIR, N^5-carboxyaminoimidazole ribonucleotide; PurK, N^5-carboxyaminoimidazole ribonucleotide synthetase; AIR, 5-aminoimidazole ribonucleotide; CAIR, 4-carboxy-5-aminoimidazole ribonucleotide; PurE, N^5-carboxyaminoimidazole ribonucleotide mutase; BC, biotin carboxylase; CPS, carbamoyl phosphate synthetase; PurT, glycinamide ribonucleotide formyltransferase (folate-independent); DDL, D-alanine:D-alanine ligase; GTS, glutathione synthetase; SynC, C-terminal domain of synapsin Ia; GAR, glycinamide ribonucleotide; PurD, glycinamide ribonucleotide synthetase; PurN, glycinamide ribonucleotide formyltransferase (folate-dependent); AMPPNP, 5′-adenylyl imidodiphosphate; PurF, phosphoribosylpyrophosphate amidotransferase.

10.1021/bi991618s CCC: $18.00
Published on Web 10/30/1999

protein interactions of the chemically unstable intermediate N^5-CAIR, may be a possibility between PurK and PurE. Second, the mechanism of the biotin-independent carboxylation catalyzed by PurK is of chemical interest as is the unprecedented migration of a CO_2 catalyzed by PurE (*5*). Third, the evolutionary link between microbial (class I) and animal (class II) PurEs, which utilize different substrates, is of interest (*2*). Recent structures of PurE (*6*) and PurK in sulfate- and MgADP-bound forms presented here provide a starting point to obtain answers to these intriguing questions.

PurK (Scheme 1) in the presence of AIR, ATP, and [^{18}O]-bicarbonate catalyzes quantitative ^{18}O transfer into [^{18}O]P_i. This observation led to the proposal that bicarbonate is activated by ATP for nucleophilic attack by the amino group of AIR through the generation of a carboxyphosphate intermediate (or its decomposition products CO_2 and P_i) (*4*). Carboxyphosphate generated from bicarbonate and ATP has also been implicated in the mechanisms of biotin carboxylases (BC) and the carbamate-forming step of carbamoyl phosphate synthetase (CPS) (*7*−*12*). Recent crystallographic studies have shown that BC and two domains of CPS are structurally homologous and part of a new superfamily of proteins containing an ATP grasp fold (*13*−*16*).

On the basis of sequence alignments, Galperin and Koonin (*17*) suggested that PurK belongs to this superfamily of proteins as well. This superfamily also includes D-alanine:D-alanine ligase (DDL), glutathione synthetase (GTS), succinyl-CoA synthetase, pyruvate phosphate dikinase, a synapsin domain (SynC), and most recently glycinamide ribonucleotide (GAR) synthetase (PurD), the second enzyme in the purine biosynthetic pathway (*18*−*22*). All of the C−N ligases in this superfamily utilize MgATP and are likely to involve phosphoanhydride intermediates.

Here we describe the three-dimensional structures of sulfate-liganded and MgADP-liganded *E. coli* PurK refined by X-ray crystallographic analysis to 2.1 and 2.5 Å resolution, respectively. As anticipated, the molecular fold of PurK is structurally homologous to the ATP grasp superfamily. A mononucleotide (AIR) binding site in PurK is proposed on the basis of conservation of PurK residues and structural homology with PurD. In turn, PurD's mononucleotide binding site was identified (*22*) by structural homology with mononucleotide-liganded PurN, the folate-dependent GAR transformylase (*23*). A comparison of PurK with other ATP grasp family members is presented.

MATERIALS AND METHODS

Protein Purification and Crystallization. PurK was purified according to a previously published procedure (*3*) with the exception that the enzyme was dialyzed against 50 mM Tris (pH 8) for 8 h at 4 °C prior to the final chromatographic step with DEAE-Sepharose. Salt and buffer levels were reduced by dilution and reconcentration with a YM30 membrane. The enzyme employed for the crystallization trials had a specific activity of 55 units/mg at 37 °C and pH 8.0 in the AIR-dependent ATPase assay where one unit is defined as 1 μmol of ADP formed/min.

For the initial sparse matrix crystallization screens of native PurK, a stock solution of enzyme (at 36 mg/mL in 10 mM Tris, pH 7.8, and 30 mM KCl) was diluted to 20 mg/mL with 10 mM PIPES (pH 7.0). These screens, which employed the hanging drop method of vapor diffusion, were conducted at both 4 °C and room temperature. Small crystals appeared at both temperatures with ammonium sulfate as the precipitant. The crystal habits were better defined at room temperature and hence the precipitant conditions were optimized at ∼22 °C. All of the crystals employed for the structural analysis of the native enzyme were grown by macroseeding into small batch setups containing 0.525 M ammonium sulfate and 100 mM HEPPS (pH 7.8). The protein concentration was typically 10 mg/mL.

Crystals of the native enzyme belonged to the space group $C222_1$ with unit cell dimensions of $a = 93.4$ Å, $b = 95.2$ Å, and $c = 120.6$ Å and one monomer per asymmetric unit. The Matthews' coefficient or V_m for these crystals was 3.4 Å^3/Da, which corresponded to a solvent content of approximately 64%.

Crystals of the enzyme/MgADP complex were grown by batch methods at room temperature as well. For these experiments, the precipitant was poly(ethylene glycol) 8000 (PEG) and the protein sample, at a concentration of 10 mg/mL, contained 100 mM HEPES (pH 7.5), 125 mM KCl, 5.0 mM $MgCl_2$, and 5 mM 5′-adenylyl imidodiphosphate (AMP-PNP) (*24*). Rod-shaped crystals typically appeared from 8−17% (w/v) PEG after 1−2 months. The crystals belonged to the space group $P1$ with unit cell dimensions of $a = 60.6$ Å, $b = 92.1$ Å, $c = 102.6$ Å, $\alpha = 66.1°$, $\beta = 82.7°$, and $\gamma = 81.8°$. The asymmetric unit contained two complete PurK dimers. Once the structure of the complex was solved, it became clear that AMPPNP had been hydrolyzed during the crystallization experiments as only MgADP remained in the active site.

Preparation of Heavy-Atom Derivatives for the Native Enzyme and X-ray Data Collection and Processing. For the preparation of heavy-atom derivatives, the native crystals were first transferred to solutions containing 0.75 M ammonium sulfate and 100 mM HEPPS (pH 7.8). Four heavy atom derivatives were readily prepared by soaking the crystals in solutions containing 1 mM methylmercury acetate for 3 h, 1 mM 2,5-bis(chloromercuri)furan for 6 h, 1 mM *meso*-1,4-bis(acetoxymercuri)-2,3-diethoxybutane for 3 h, or 10 mM K_2PtCl_4 for 60 h. X-ray data from the native and heavy-atom derivative crystals were collected at −2.5 °C with a Bruker AXS HiStar area detector system. The X-ray source was Ni-filtered Cu Kα radiation from a Rigaku RU200 X-ray generator operated at 50 mV and 90 mA and equipped with double focusing mirrors. Only one crystal was required for each X-ray data set to 2.7 Å resolution. Friedel pairs were measured for each of the heavy-atom derivative *x*-data sets. All data sets were processed with the software package XDS (*25*, *26*) and internally scaled with the program XCALIBRE (G. Wesenberg and I. Rayment, unpublished software). Relevant X-ray data collection statistics are given in Table 1. The heavy-atom derivative data sets were scaled to the native by a "local" scaling procedure developed by Drs. G. Wesenberg, W. Rypniewski, and I. Rayment. The *R*-factors (based on amplitudes) between the native and the methylmercury acetate, 2,5-bis(chloromercuri)furan, *meso*-1,4-bis(acetoxymercuri)-2,3-diethoxybutane, and K_2PtCl_4 data sets were 23.9%, 15.7%, 16.8%, and 18.8%, respectively. Once the structure had been determined to 2.7 Å resolution, a final native X-ray data set was collected to 2.1 Å resolution by using three crystals. This particular data set

Table 1: Data Statistics

data set	resolution (Å)	independent reflections	completeness (%)	avg I/avg σ (I)	R_{sym}[a] (%)	R_{iso}[b] (%)	phasing power[c]
native I	30−2.7	14 589	96.4	31.5	4.3		
methylmercury acetate	30−2.7	14 719	97.3	13.6	5.6	23.9	1.06
2,5-bis(chloromercuri)furan	30−2.7	14 492	95.8	10.4	6.8	15.7	1.30
meso-1,4-bis(acetoxymercuri)-2,3-diethoxybutane	30−2.7	13 726	90.7	13.2	4.6	16.8	1.10
K_2PtCl_4	30−2.7	14 000	92.5	8.3	6.3	18.8	1.30
native II	30−2.1	30 332	95.6	24.3	4.7		
Mg^{2+}ADP complex	30−2.5	66 345	95.7	12.6	7.2		

[a] $R_{sym} = (\sum|I - \langle I\rangle|/\sum I) \times 100$. [b] $R_{iso} = (\sum|F_h| - |F_n|)/\sum_n F_n \times 100$, where F_h and F_n are the heavy atom and native structure factors, respectively. [c] Phasing power is the ratio of the root-mean-square heavy-atom scattering factor amplitude to the root-mean-square lack of closure error.

was processed with the data reduction software package SAINT (Bruker AXS INC) and internally scaled with XCALIBRE. The X-ray data set was 95.6% complete to 2.1 Å resolution. Relevant statistics for this data set are also presented in Table 1. X-ray data from a single crystal of the PurK/MgADP complex were collected in a manner similar to that described above and processed with SAINT and XCALIBRE. Relevant statistics are given in Table 1.

Structural Determination and Least-Squares Refinement of the Native PurK. The positions of the heavy atom binding sites were determined by inspection of difference Patterson maps calculated with X-ray data from 30 to 5.0 Å. The methylmercury acetate, 2,5-bis(chloromercuri)furan, *meso*-1,4-bis(acetoxymercuri)-2,3-diethoxybutane, and K_2PtCl_4 derivatives contained two, six, one, and five heavy-atom binding sites, respectively. The heavy-atom derivatives were placed on a common origin by difference Fourier maps and the positions and occupancies for each heavy-atom binding site were refined by the origin-removed Patterson-function correlation method to 2.7 Å resolution (*27*, *28*). All the mercury-based derivatives had one common binding site near Cys 5, but the exact locations of these heavy atoms were not identical. Anomalous difference Fourier maps calculated from 30 to 5.0 Å were employed for determining the correct hand of the heavy-atom constellation. Protein phases were calculated with the program HEAVY (*27*) and relevant phase calculation statistics can be found in Table 1.

An electron density map calculated to 2.7 Å resolution clearly revealed the overall course of the polypeptide chain. The map was subsequently improved by the technique of solvent flattening (*29*) as implemented by Dr. W. Kabsch, Heidelberg, Germany. From the density-modified map it was possible to trace the entire polypeptide chain contained within the asymmetric unit. The PurK subunit contains 355 amino acid residues (*30*, *31*). There was one break in the protein backbone delineated by Thr123−Gly130. Additionally, in the final electron density map the side chain corresponding to Phe41 was disordered with only enough electron density to accommodate an alanine residue. According to the published amino acid sequence, residue 205 is a glutamine (*30*, *31*). The electron density map, however, clearly revealed the presence of an arginine at position 205 that forms a salt bridge with Glu208. Resequencing of the DNA confirms this assignment. The model was refined by least-squares analysis to 2.1 Å resolution with the software package TNT (*32*). Relevant refinement statistics are given in Table 2. The final *R*-factor was 19.6% for all measured X-ray data from 30 to 2.1 Å resolution. In addition to *R*-factor values and the overall geometry of the model, perhaps one of the strongest indications of model quality is a plot of the polypeptide chain backbone dihedral angles. A Ramachandran diagram of such torsional angles is presented in Figure 1A, and as can be seen there are no significant outliers. A representative portion of the electron density map near the region surrounding the observed sulfate anion is given in Figure 1B. In addition to this sulfate ion, there were 92 water molecules included in the refinement and these had an average *B*-value of 49.0 Å^2. The average *B*-value for the polypeptide chain backbone atoms was 41.7 Å^2.

Table 2: Least-Squares Refinement Statistics

	PurK/sulfate complex	PurK/MgADP complex
resolution limits (Å)	30.0−2.1	30.0−2.5
R-factor[a] (%)	19.6	18.5
no. of reflections used	30 332	66 345
no. of protein atoms	2737	11137
no. of solvent atoms[b]	97	495
Weighted Root-Mean-Square Deviations from Ideality		
bond length (Å)	0.013	0.013
bond angle (deg)	2.33	2.23
planarity (trigonal) (Å)	0.005	0.006
planarity (other planes) (Å)	0.011	0.013
torsional angle[c] (deg)	17.6	19.3

[a] *R*-factor $= \sum|F_o - F_c|/\sum|F_o|$, where F_o is the observed structure-factor amplitude and F_c is the calculated structure-factor amplitude. [b] These include 92 waters and one sulfate ion in the native model and 491 waters and four magnesium ions in the complex model. [c] The torsional angles were not restrained during the refinement.

Structural Determination and Least-Squares Refinement of the PurK/MgADP Complex. The structure of the PurK/MgADP complex was solved by molecular replacement with the software package AMORE (*33*) with the native PurK dimer employed as a search model. A search sphere radius of 25 Å was utilized. Both the cross-rotational functions and translational searches were conducted with X-ray data from 20 to 4.0 Å. Two solutions were obtained corresponding to the two dimers in the asymmetric unit. Following rigid-body refinement with X-ray data from 20 to 4.0 Å, the correlation coefficient was 65.3% and the *R*-factor was 38.9%. To expedite the model building process and to remove bias due to the molecular replacement technique, the four subunits in the asymmetric unit were averaged according to the algorithm of Bricogne (*34*). From this averaged electron density map, one subunit of the PurK/MgADP complex was constructed. This averaged model was placed back into the unit cell and subjected to alternate cycles of least-squares refinement and model building. Relevant refinement statistics are given in Table 2. In each subunit, there was an intramolecular disulfide bridge between Cys146 and Cys150.

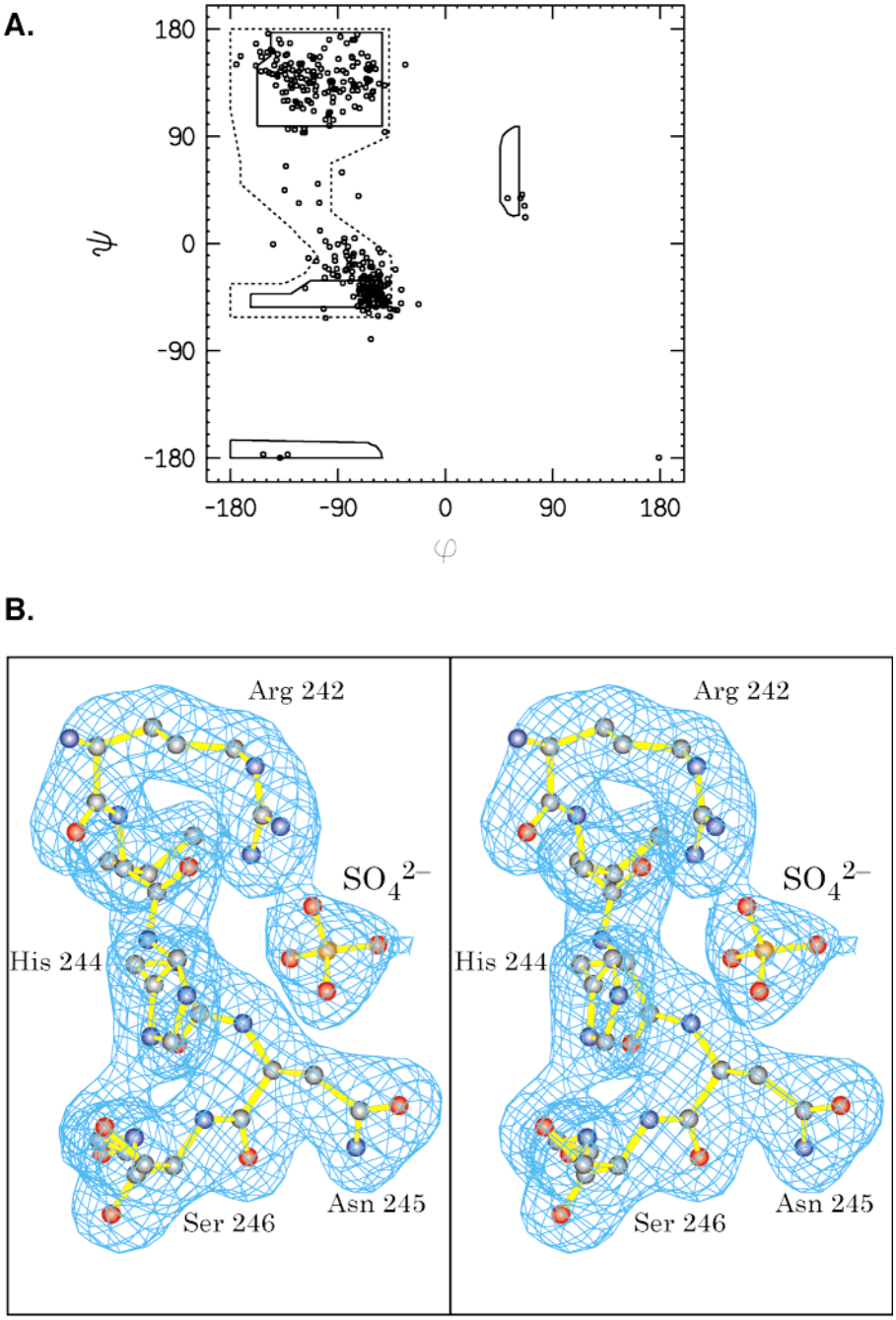

FIGURE 1: Quality of the X-ray model for native PurK. (A) One of the more important assessments of model quality is the appearance of the Ramachandran plot. Shown here is a plot of all nonglycinyl main-chain dihedral angles for the PurK subunit. Fully allowed ϕ,ψ values are enclosed by solid lines; those partially allowed are enclosed by dashed lines. (B) A portion of the final electron density map for PurK is displayed. The map was contoured at 3σ and calculated with coefficients of the form $(F_o - F_c)$, where F_o was the native structure factor amplitude and F_c was the calculated structure factor amplitude. Both the sulfate ion and the region of polypeptide chain from Arg 242 to Gly 274 were removed from the coordinate file employed in the map calculation.

A Ramachandran plot of all nonglycinyl main-chain dihedral angles is displayed in Figure 2A, and electron density corresponding to the nucleotide in subunit II of the asymmetric unit is shown in Figure 2B.

RESULTS AND DISCUSSION

Tertiary and Quaternary Structure of the Native PurK. A ribbon representation of a single subunit of PurK is displayed in Figure 3A. The architecture of the monomer, with overall dimensions of approximately 55 Å × 60 Å × 62 Å, can be envisioned in terms of three structural motifs referred to as the A, B, and C domains. This nomenclature was originally employed to describe the three-dimensional models for both BC and CPS and thus is retained here (*13, 14*). In PurK, the A, B, and C domains extend from Met1 to Ala95, from Pro96 to Ser159, and from Gly160 to Gly355, respectively. The B domain is separated from the A and C domains and is thermally more flexible. Dimer formation is mediated by the A and C domains (Figure 3B). The secondary structural elements assigned to each domain according to both the results from DSSP (*35*) and visual inspection of the model are given in Figure 4.

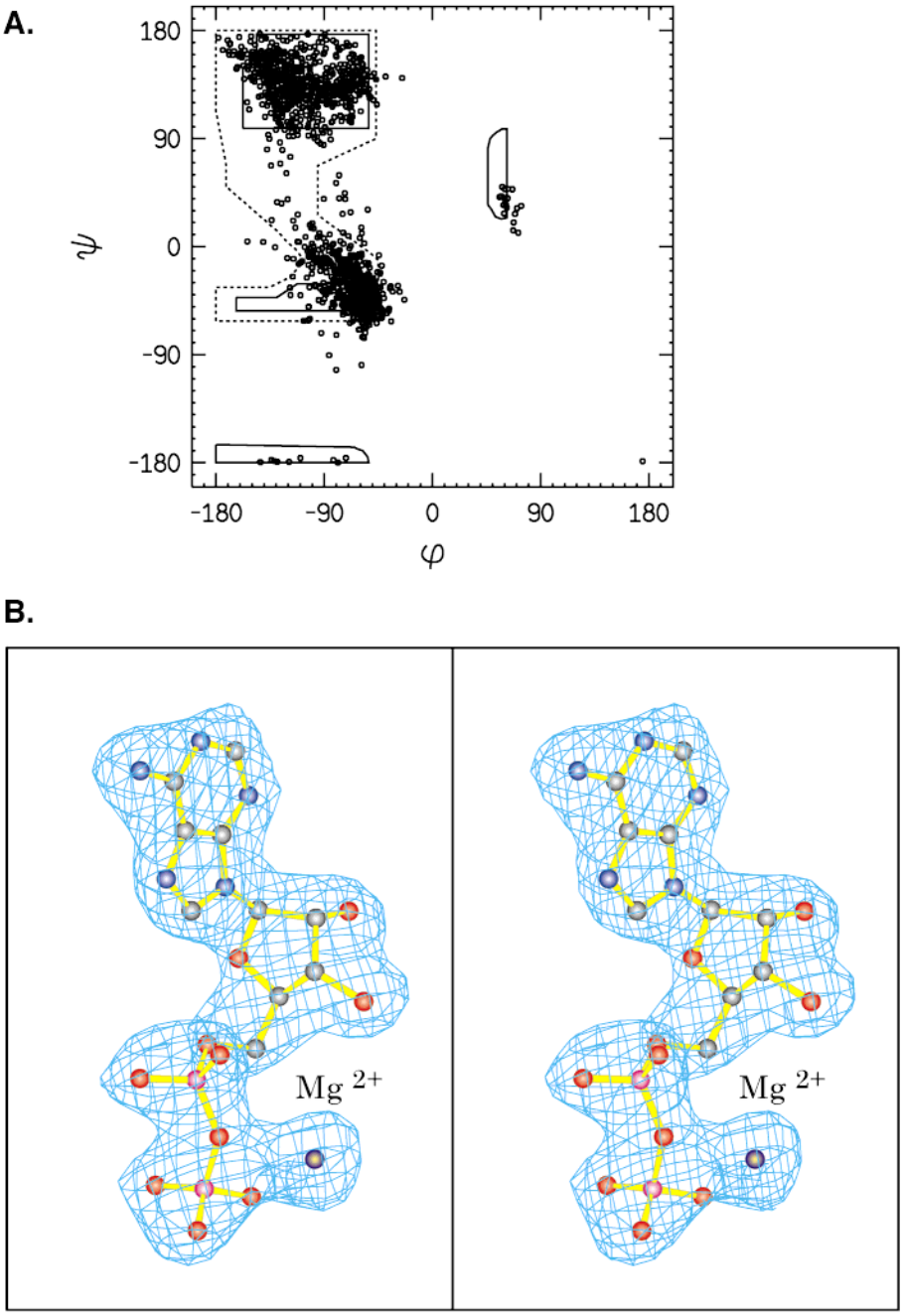

FIGURE 2: Quality of the X-ray model for the PurK/MgADP complex. Shown in panel A is a plot of all nonglycinyl main-chain dihedral angles for the four subunits of PurK contained within the asymmetric unit. Electron density corresponding to the nucleotide in subunit II is displayed in panel B. The map was contoured at 3σ and calculated with coefficients of the form ($F_o - F_c$), where F_o was the native structure factor amplitude and F_c was the calculated structure factor amplitude. The nucleotide was not included in the coordinate file employed for the map calculation.

The A-domain contains three strands of parallel β-sheet that range in length from four to seven residues and four distinct α-helical regions composed of 5−10 amino acids. Additionally, there are numerous classical reverse turns connecting these secondary structural elements. The molecular axes of the third (Phe74−Ala78) and fourth (Arg80−Phe87) α-helices in the A-domain are oriented at approximately 90° with respect to one another and are connected by one residue, Asp 79, which adopts dihedral angles of $\phi = -95.0°$ and $\psi = 119.8°$. This type of tertiary pattern, namely, a helix−residue−helix motif, appears to be a structural hallmark for enzymes belonging to the ATP grasp superfamily of proteins and serves as the bridge between the A- and B-domains. Similar dihedral angles are observed for the single connecting residues between the equivalent two α-helices in DDL (Asp96, $\phi = -103°$, $\psi = 104°$), GTS (Asn 123, $\phi = -70°$, $\psi = 142°$), BC (Asp 115, $\phi = -113°$, $\psi = 95°$), both synthetase domains of the large subunit of CPS (Asp 128, $\phi = -81°$, $\psi = 121°$, and Asp 674, $\phi = -84°$, $\psi = 119°$), and PurD (Ser 104, $\phi = -123°$, $\psi = 111°$).

A structural homology search of the Brookhaven Protein Data Bank using the A domain of PurK and the program DALI (*36*), revealed many Rossmann fold-containing proteins including the N-terminal domain of the third enzyme in the purine biosynthetic pathway: GAR formyltransferase

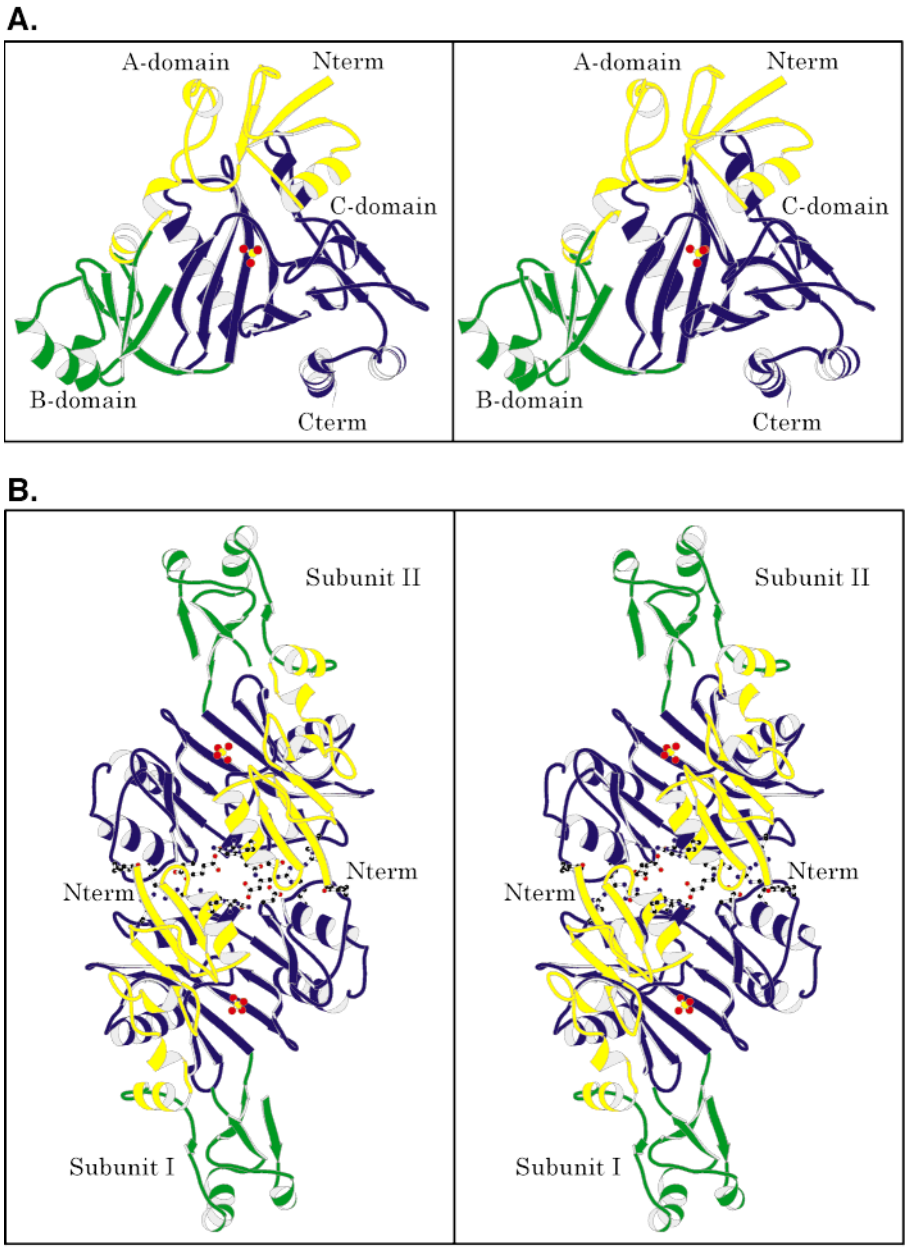

FIGURE 3: Tertiary and quaternary structure of PurK. A single PurK subunit is shown in panel A. The A, B, and C domains of the subunit are color-coded in yellow, green, and blue, respectively. A sulfate molecule observed in the electron density map is displayed in a ball-and-stick representation. The ribbon representation of the PurK dimer shown in panel B is oriented perpendicular to the crystallographic *a*-axis. Those amino acid side chains involved in electrostatic interactions within the subunit−subunit interface are depicted as ball-and-sticks.

(PurN) and the A domain of PurD.[2] The structure of PurN has been solved in the presence of GAR (*23*). The structural homology of PurN with PurK and PurD allows an excellent guess about the mononucleotide (AIR and N^5-CAIR) binding site on PurK. The phosphate is proposed to interact with the P loop (G_8−L_{12}) of the N-terminal strand loop helix (Figures 3A and 4B). The P loop region consensus by alignment of 22 full-length PurK sequences is G_8[G/N/D]GQL_{12}. This loop appears to provide the flexibility for phosphate binding and stabilization by the adjacent helix α1 dipole. A similar mononucleotide binding motif has been established structurally for two additional enzymes in the purine pathway: PurF (*37*) and recently PurE (*6*). Thus five of the 11 enzymes in this pathway have a similar binding site for a ribose 5-phosphate moiety, common to all intermediate metabolites in this pathway.

The B-domain, depicted in green in Figure 3A, contains four strands of antiparallel β-sheet ranging in length from three to nine amino acid residues (Figure 4B). This β-sheet is flanked on one side by two α-helices formed by Arg103−Leu113 and Ala136−Gln141. The second helix in this domain (α6) is decidedly distorted due to Glu138, which adopts dihedral angles of $\phi = -84.6°$ and $\psi = 3.6°$. The region of polypeptide chain from Thr123 to Gly130 is disordered in the present structure and is referred to as the B loop. In 24 full-length or partial PurK sequences, the B loop consensus sequence is X_{123}X[G/A]YDG[R/K/Q/H]G_{130}.

[2] The A domain of PurD was referred to as the N domain in the previous paper (*22*).

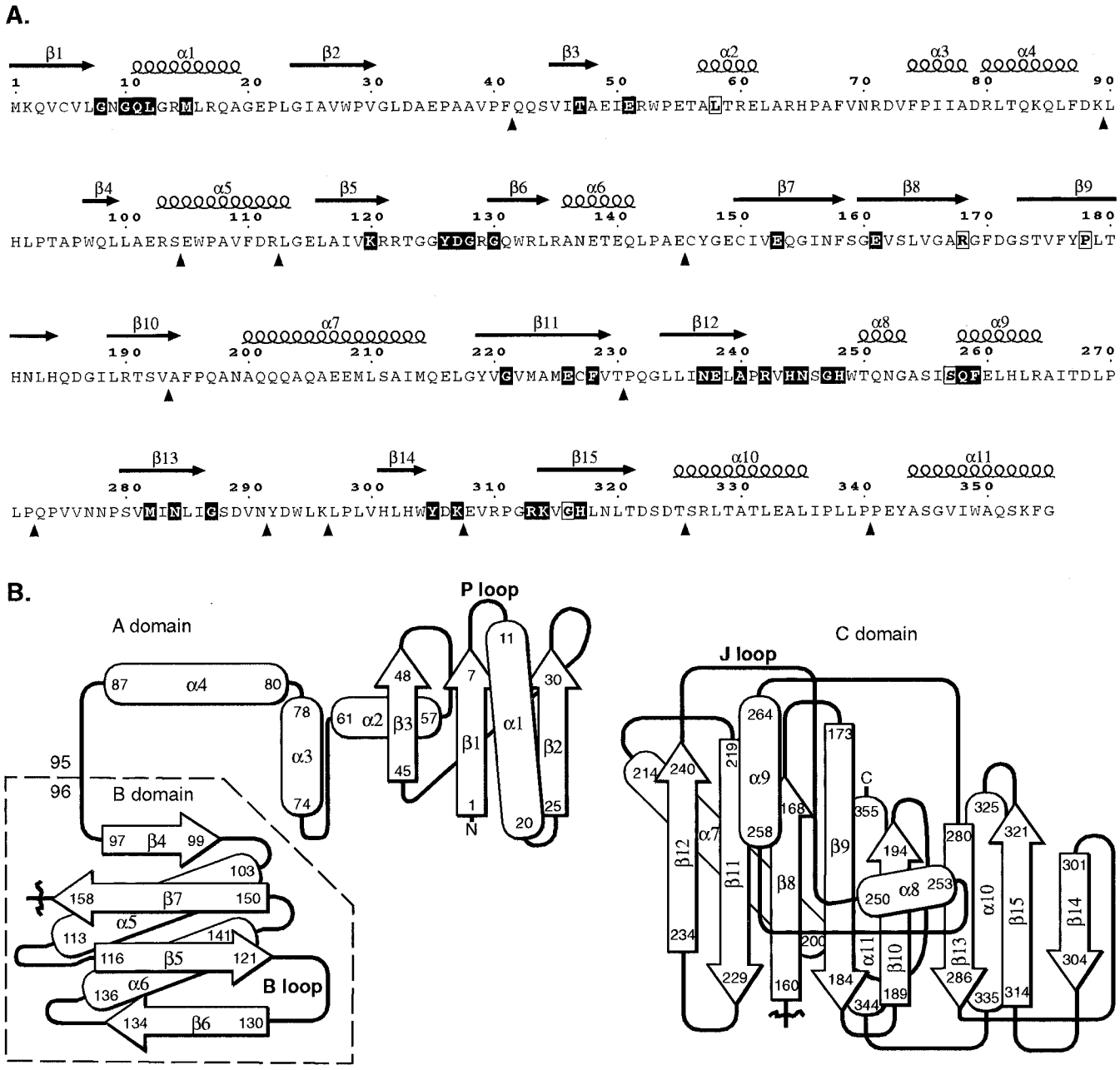

FIGURE 4: Secondary structure and strictly conserved amino acid residues in PurKs. (A) Sequence of *E. coli* PurK. The white letters in black boxes are conserved among 22 full-length PurK sequences. Black letters in white boxes are conserved among 21 PurK sequences. Triangles indicate where any insertion is required in the *E. coli* sequence to generate the indicated consensus sequence. (B) Topology diagram of the secondary structure of the A, B, and C domains of PurK. For clarity, the linker between β7 and β8 is not shown, and the C domain has been moved to the right of the A and B domains.

All members of the ATP grasp superfamily whose structures have been determined in the absence of a ligand have disordered B loops. In the case of the available nucleotide liganded structures these B loops are generally ordered. Structural alignments of these loops, which are in general Gly- and Ser-rich, reveal that the PurK B loop has one additional residue (Figure 5A). In the available liganded structures, the amide hydrogens of the two C-terminal residues [M*GG* or G*SS*, △ and ▲ in Figure 5A] participate in hydrogen-bonding interactions with the β- and γ-phosphate groups of the nucleotide. In PurK the corresponding sequence $Y_{126}DG_{128}$ is unique in that one side chain is large and another is charged. In the structure of sulfate-liganded PurK, Tyr126 makes an unusual salt bridge with Arg129. Asp127 might function as a metal ligand, as discussed below. Most members of the ATP grasp superfamily also possess a second loop (called the Ω loop, Figure 6A) in their C domain that interacts with the B loop, providing a protective face over the β- and γ-phosphates of ATP and the putative acyl phosphate intermediate. As noted below, this Ω loop is very short in the PurK structure. Hence the Tyr and Asp of PurK's B loop may play an important role in sequestration of the active site in conjunction with conserved residues including the J loop (Ala240−His244) of the C domain (Figure 6, discussed subsequently).

The C-domain, the most complicated of the three domains (Figures 3A and 4B), is dominated by a twisted eight-stranded antiparallel β-sheet that forms a basket to cradle the A- and B-motifs. These β-strands range in length from 4 to 11 amino acids with an average length of eight residues.

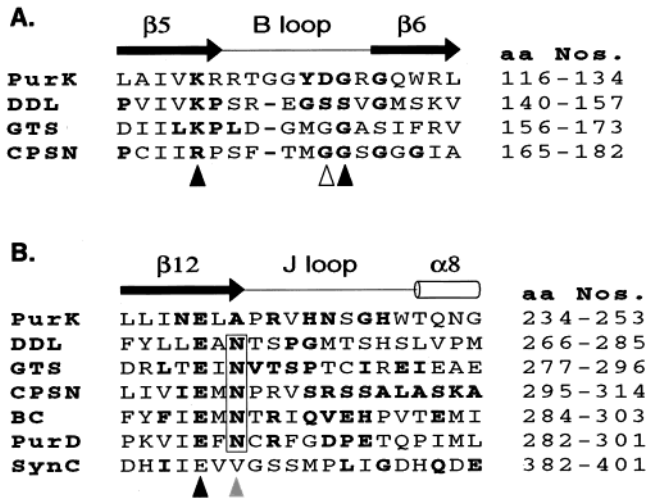

FIGURE 5: Comparison of B loop and J loop consensus sequences from a structure-based alignment of four ATP grasp proteins. In each panel, secondary structure assignments from PurK are indicated. Boldface residues are positions conserved within each enzyme. Sequence ranges are indicated (*E. coli* numbering, except SynC from *B. taurus*). A sequence from the N-terminal carbamate-generating domain from the large subunit of CPS is shown (CPSN). (A) Comparison of B loop sequences in four ATP grasp proteins with structures where a nucleotide is bound and the B loop is visible. Solid triangles indicate positions observed to contact ADP, and the open triangle indicates a position expected to make a backbone NH contact with the β- and γ-phosphates in ATP. (B) Comparison of J loop sequences in six crystallographically characterized ATP grasp enzymes. The solid triangle is a ligand to metal 1, and the shaded triangle is a ligand to metal 2 in some enzymes (boxed Asn residues).

The third, fourth, and fifth β-strands (β10−β12) are interrupted by bulges resulting from the dihedral angles adopted by Arg 190 ($\phi = -115.4°$, $\psi = -37.6°$), Gly 221 ($\phi = 125.9°$, $\psi = -163.4°$), and Asn 237 ($\phi = -98.3°$, $\psi = -64.6°$). There are also four α-helices and numerous regions of reverse turns distributed throughout the C-domain.

The C domain varies in size and complexity among members of the ATP grasp superfamily (*22*). However, in all of the structurally well-characterized proteins, the C-domain J loop provides a structurally conserved strand−loop structure (Figures 5B and 6C) that cradles the ATP. It is called a J loop because of the strand−loop structure's shape: the loop hooks to the right as it extends from β12. The conservation of residues within this motif is high within enzymes but not among superfamily members. The conserved residues in PurK are shown in boldface type (Figure 5B), as are the conserved residues within other members of this superfamily. Several conserved features from PurK are important to note: Arg242 interacts electrostatically with two of the oxygens of the sulfate from the sulfate-liganded PurK. The sulfate also interacts with the backbone amide of conserved Asn245. Glu238 is conserved not only within PurKs but among all of the members of this superfamily. From the Mg-nucleotide liganded structures available (*20*, *38*), this Glu is known to be a metal ligand. One feature that is strikingly different between PurK and the other superfamily members is Ala240. This residue is an Asn and a known metal ligand in the other family members, except SynC.[3] In the case of PurK, portions of the C domain including this J loop and the P loop from the A domain, unique to the purine enzymes, form the binding pocket for the mononucleotide substrate AIR and will be discussed subsequently.

The differences in complexity of the C domains of the superfamily members are most apparent in the region C-terminal to the J loop. In DDL, GTS, SynC, and the two domains of CPS, the J loop is near the end of the C domain. In PurK, PurD, and BC, an additional globular feature follows the J loop (residues 247−355 in PurK). In the case of PurK this feature appears to contribute a significant portion of the AIR binding site. A comparison of all of the structures of this superfamily reveals that, aside from the protein topology, the J loop is the only common feature in the C-domain.

Dimer Interface of PurK. PurK is known to function as a dimer in solution (*3*). In the crystals employed in this investigation, the dimeric protein is packed in the unit cell with its molecular dyad coincident with a crystallographic 2-fold, thereby leading to an asymmetric unit containing only one subunit. Shown in Figure 3B is a ribbon representation of the PurK dimer viewed perpendicular to the crystallographic *a*-axis. The dimer has overall dimensions of approximately 55 Å × 95 Å × 88 Å and a subunit−subunit buried surface area of 2850 Å^2 as calculated according to the method of Lee and Richards (*40*) with a probe sphere of 1.4 Å. For comparison, the buried surface area of BC, also known to be a dimer and similar in structure to PurK, is 2600 Å^2 (*13*). The specific manners by which the subunits of PurK and BC associate to form functional dimers, however, are quite different even though in both cases the B-domains extend away from the main bodies of the proteins. PurD and PurT (a formate-dependent GAR transformylase), members of this superfamily and of the purine biosynthetic pathway, are monomers (*41*, *42*).

There are four specific regions of polypeptide chain in each PurK subunit that are involved in maintaining the proper quaternary structure of the protein. One of these regions in subunit I of the dimer involves those residues lying in the first α-helical region of the A-domain as can be seen in Figure 3B. Here there are numerous hydrogen bonds between the two subunits including those formed by O of Pro22 (subunit I) and N of Trp304 (subunit II), O of Leu23 (subunit I) and O$^\eta$ of Tyr292 (subunit II), and N$^{\epsilon 2}$ of Gln18 (subunit I) and O$^{\epsilon 1}$ of Glu21 (subunit II). Additionally, there is a salt bridge formed between the guanidinium group of Arg17 (subunit I) and the carboxylate group of Glu21 (Subunit II). The second region of subunit−subunit contact occurs in the area delineated by Ser255 and Asn277. Specific electrostatic interactions are formed between O$^\gamma$ of Ser255 (subunit I) and O of Pro289 (subunit II), N$^{\eta 2}$ of Arg264 (subunit I) and O of Leu295 (subunit II), N$^{\delta 2}$ of Asn277 and O$^{\delta 2}$ of Asp322, and O$^{\delta 1}$ of Asn277 (subunit I) and N$^{\eta 2}$ of Arg327 (subunit II). By the local symmetry of the dimer, the third and fourth areas of contact provided by subunit I are necessarily formed by Tyr292−Asp306 and Asp322−Arg327. In addition to these specific electrostatic interactions, there are numerous water molecules distributed throughout the subunit−subunit interface.

Location of the Active Site of PurK. As noted above, the structures of MgADP and sulfate-liganded PurK define part of its active-site cleft. Additional insight into the active site,

[3] A crystal structure of SynC contains Ca^{2+} and ATP (*39*). The function of this synapsin and whether ATP is hydrolyzed remain unknown.

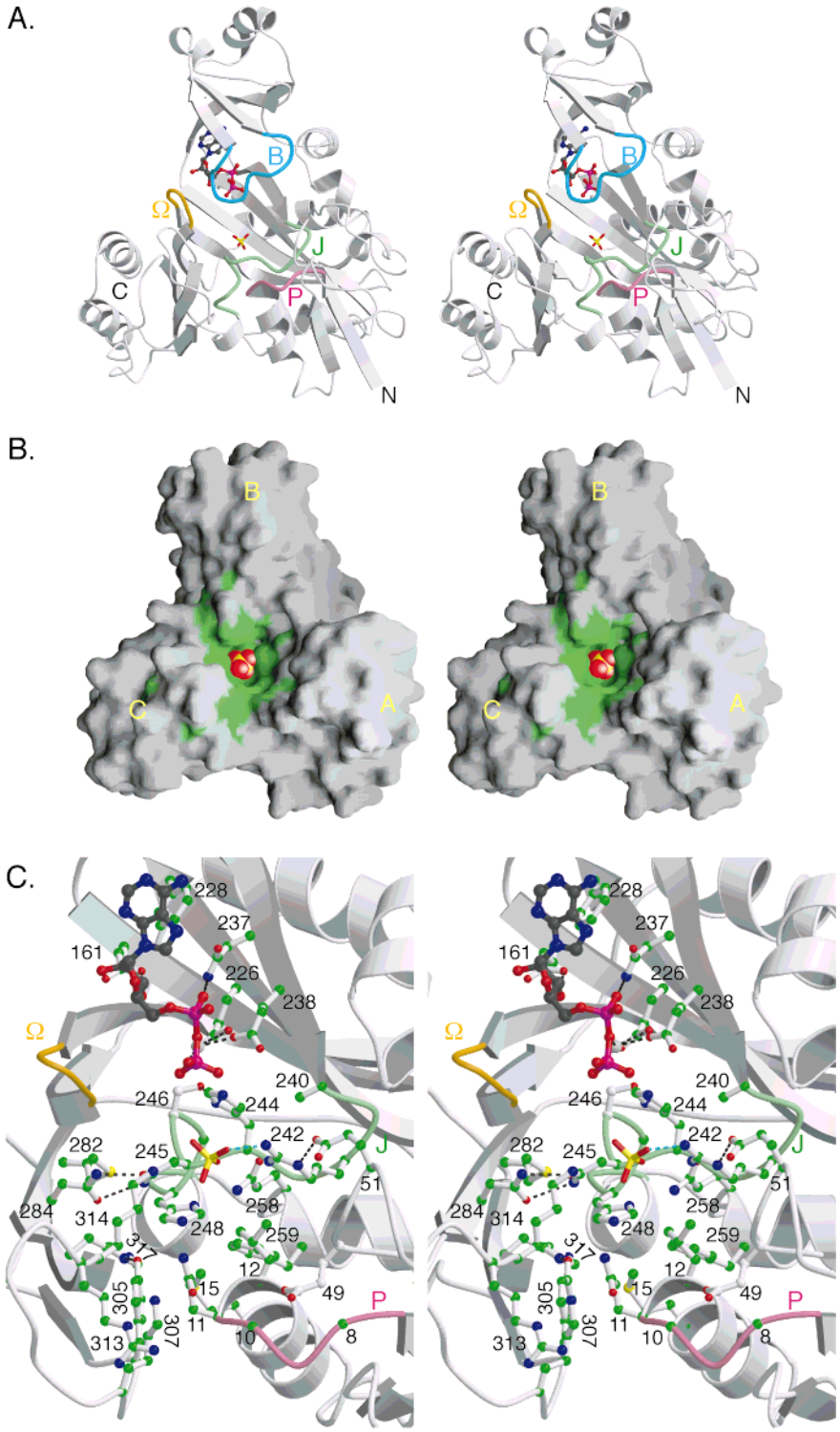

FIGURE 6: Active site of PurK. (A) Close-up showing the B loop (blue), the Ω loop (yellow), the P loop (red), and the strand-J loop (green) using the MgADP structure. Both sulfate and the MgADP are shown. The sulfate has been superimposed on the MgADP structure. (B) Molecular surface of PurK in the same orientation as in panel A. Surface-exposed conserved residues are colored green and the sulfate binding site is shown (CPK model); in this view MgADP is mostly obscured by the B loop. This view provides a glimpse at the putative AIR binding pocket. The figure was prepared with GRASP (*50*). (C) Closer view of the structure in panel A with the conserved residues labeled. All of the conserved residues (Figure 4A) within the active site are depicted in ball-and-stick representations. The partially conserved Glu49 (Asp) and Ser247 (Thr) are shown with white C atoms. The view is tilted forward 45° relative to the view in panels A and B, and the B domain has been removed for clarity. Panels A and C were prepared with Molscript (*51*) and Raster3D (*52*).

including the AIR binding site, is provided by the location of the 34 strictly conserved residues of ~355 amino acids of PurK in 22 full-length sequences available (Figure 6). As shown in Figure 5, the B loop region in the B domain and the strand−J loop in the C domain contain five and eight conserved residues, respectively. In addition, the P loop and the adjacent helix α1 (five conserved residues) in the A domain are proposed to bind the phosphate of AIR and provide part of AIR's binding pocket. The remainder of AIR's binding pocket is proposed to be provided by nine of

the 10 conserved residues in the C-terminus of the C domain (i.e., after the J loop in primary sequence, Figure 4A). This region nuzzles up against the P-loop helix α1 in the A domain and together they are proposed to form the AIR binding pocket. A picture of the putative AIR binding pocket with the B domain removed for clarity is shown in Figure 6C.

Carboxyphosphate Binding Site. The sulfate binding site of the sulfate-liganded PurK could be indicative of the γ-phosphate binding site of ATP, the binding site of the product phosphate, or the phosphate binding site of the mononucleotide substrate, AIR. As discussed above, we believe that the phosphate binding site of the mononucleotide resides in the A domain. Thus this last possibility seems unlikely. A clue as to the function of the sulfate binding site in PurK may be provided by the phosphate-liganded structures of BC and the carbamate-forming domain of CPS. In these proteins, the phosphate ions are located in nearly identical positions to the sulfate in PurK and interact with an Arg side chain and a backbone amide group [Arg292 and Val295 in BC (*13*); Arg303 and Arg306 in CPS (*43*)]. Since the reaction mechanisms of PurK, BC, and the carbamate-forming domain of CPS all require bicarbonate and are thought to proceed through a carboxyphosphate intermediate, one can speculate that this site is involved in binding bicarbonate and/or the carboxyphosphate intermediate.

MgADP and MgATP Binding Site. In attempt to more clearly define the ATP binding site of PurK, crystals of the enzyme complexed with MgAMPPNP were prepared and the structure solved. As described in the Materials and Methods section, the crystals belong to the space group *P*1 and contained four complete subunits in the asymmetric unit. For the sake of simplicity, only subunit II is discussed here since the electron density corresponding to this polypeptide chain is the best-ordered.

AMPPNP was chosen for cocrystallization due to its presumed stability in the absence of the AIR. In fact, during the course of the crystallization experiments, the ligand was hydrolyzed to MgADP as can be seen in Figure 7 (*18*). From a detailed structural analysis of CPS, it is known that the B-domains in the large subunit of the enzyme close down tightly when either AMPPNP (and presumably ATP as well) or ADP/P_i is bound in the active sites (*15, 16*). Indeed, the trigger for the B-domain closure in CPS appears to be the formation of hydrogen bonds between the γ-phosphates of the nucleotide moieties and the backbone amide nitrogens of glycine residues occupying the second and third positions in type III′ reverse turns in the B loop. Strikingly, some of the atoms in the B-domains of CPS move by more than 7 Å (*16*). This transformation of the B loop from a disordered to an ordered state concomitant with a conformational change has also been observed for GTS, for which both open and closed structures of this protein are available (*21, 38*).

Since only MgADP is observed binding in the PurK active site, rather than a combination of nucleoside diphosphate and inorganic phosphate, the B-domain closure is not as extensive as that observed in CPS or GTS. Still, there is significant movement with some atoms moving by more than 3.0 Å, as can be seen in Figure 8. The major structural differences between the two forms of PurK presented here are confined to a region within the B domain, residues Leu100−Val152. Excluding this region, however, the polypeptide chains for the two models are remarkably similar, such that their backbone atoms superimpose with a root-mean-square deviation of 0.43 Å. The actual conformation of the B loop may change further upon binding of a Mg-nucleoside triphosphate.

Shown in Figure 7 is a close-up view of that portion of the PurK active site responsible for positioning the nucleotide. The adenine ring is linked to the protein via a hydrogen bond to N-1 contributed by the backbone amide group of Ile156 and packed against a hydrophobic pocket formed by Ile156 and Phe158. In addition, the 6-amino group appears to be hydrogen-bonded to the carbonyl of Glu154 and one of the carboxylate oxygens of Glu153. The ribose ring adopts a $C_{3'}$-*endo* pucker with its 2′- and 3′-hydroxyl groups lying within hydrogen-bonding distance of the carboxylate side chain of Glu161. Arg80 interacts electrostatically with the α- and β-phosphates of ADP, and Lys120 interacts with the α-phosphate and adenine N-7. At a resolution of 2.5 Å it is not possible to unambiguously define the coordination geometry around the putative Mg ion observed in the electron density map for PurK. In PurK, Mg is ligated by a phosphoryl oxygen and a bridging oxygen from the nucleotide, $O^{\epsilon 1}$ and $O^{\epsilon 2}$ of Glu226 and $O^{\epsilon 2}$ of Glu238. While the definition of the coordination geometry will change upon refinement of the model at higher resolution, it is clear that both Glu226 and Glu238 act as ligands to the metal ion.

The availability of several high-resolution structures of members of the ATP grasp superfamily with MgADP and MgATP bound allow similarities and differences in the nucleotide binding site to be discussed. In almost all cases either the 2′ or 3′ hydroxyls of the ribose of ADP or ATP are bound to a conserved Glu (Glu161 in PurK). In most structures either one or two Mg or Mn ions interact with the β- and γ-phosphates of the nucleotides with two conserved metal ion binding residues in the strand−J loop region: EXN (Figure 5B). For no ATP grasp enzyme is a detailed understanding of the role of the metal(s) in catalysis available. As we discussed above, the first metal binding motif in PurK is $E_{238}XA_{240}$, raising the possibility that there may not be a second metal binding site in PurK, which would be a unique situation for an ATP grasp enzyme known to hydrolyze ATP.[3] Asp 127, a conserved residue at the tip of the B loop, is near the ADP β-phosphate (Figure 7) and might function as a ligand to a second metal.[4]

In most superfamily members, the charges on the phosphates of the nucleotide are in part neutralized by three positively charged Lys or Arg residues: one from the A domain helix−residue−helix kink (Arg80 in PurK), one from the underside of the B domain (Lys120 in PurK), and one from the Ω loop.[5] PurK differs from other ATP grasp enzymes in that a third positive charge is not present. Given that there is a lower positive charge around the reactive end of ATP and a perturbed metal binding motif, there may be significant differences in the activation of ATP by PurK.

AIR/N^5-CAIR Binding Site. There is no definitive evidence for the mononucleotide (AIR) binding site. Recent structures of nucleotide-bound PurF, PurN, and PurE exhibit a common

[4] A residue in the B loop of human GTS, a circularly permuted analogue of *E. coli* GTS, functions as a ligand to the second Mg in a recent structure with ADP, sulfate, two Mg ions, and glutathione bound at the active site (*44*).

[5] In both ATP grasp domains in CPS, the third charge is an Arg at the junction between the J-loop and the subsequent helix.

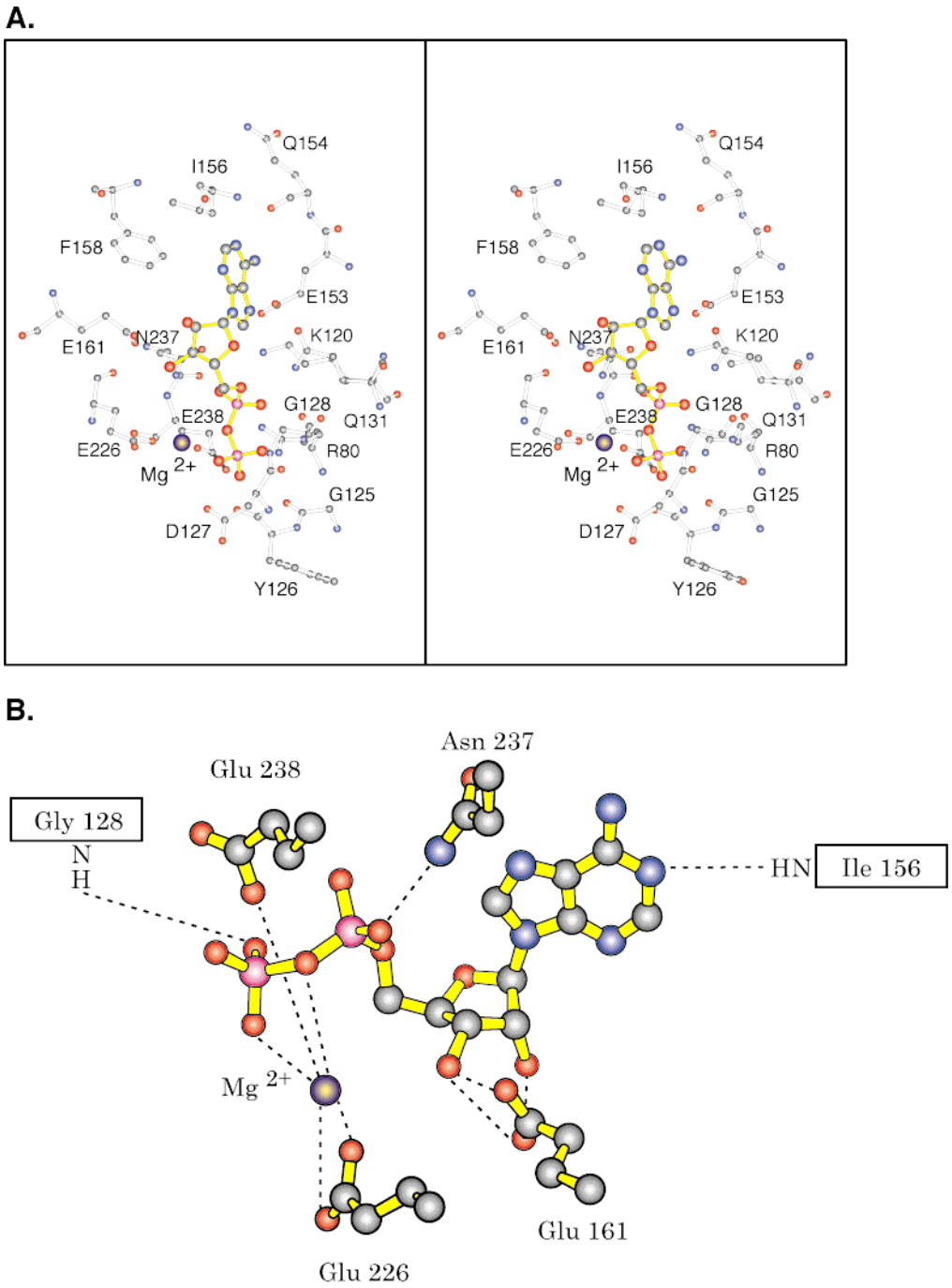

FIGURE 7: Nucleotide binding pocket of PurK. A close-up view of the region surrounding the MgADP moiety is shown in panel A. A cartoon of the potential electrostatic interactions between the nucleotide and the protein, within approximately 3.0 Å, is depicted in panel B. The dashed lines indicate possible hydrogen bonds. The hydrogen-bonding pattern most likely will change when the structure of the PurK/MgADP complex is refined to higher resolution.

strand−loop (P loop)−helix binding and stabilizing the phosphate of ribose 5-P (*6*, *23*, *37*). PurK contains a similar motif, suggesting the mononucleotide binding site. Examination of the MgADP and sulfate binding sites reveals that this putative mononucleotide binding site is in an appropriate position given the chemistry of the reaction (Figure 6A,C). In the structures of PurN and PurE there are carboxylates positioned to bind one or both hydroxyls of the ribose moiety of the mononucleotide. Several residues in the A domain of PurK are candidates for a similar function: Glu51 (conserved) and Glu 49 (semiconserved, an Asp in two sequences). One of the carboxylate oxygens in Glu51 forms a hydrogen bond with N^{ϵ} of Arg242 in the MgADP−PurK structure, which is disrupted in the sulfate−PurK structure. As a result, the position of the Glu51 side chain is one of the larger differences between the sulfate- and MgADP-liganded PurK structures. Whether Glu51 could assist in mononucleotide binding as observed in the other purine mononucleotide binding proteins remains to be determined. Alternatively Glu49, which in the present structures makes a favorable interaction with the helix α1 dipole in the P loop structure, might undergo a conformational change to allow phosphate binding and be positioned to facilitate ribose binding. In either case, it appears necessary for the loop

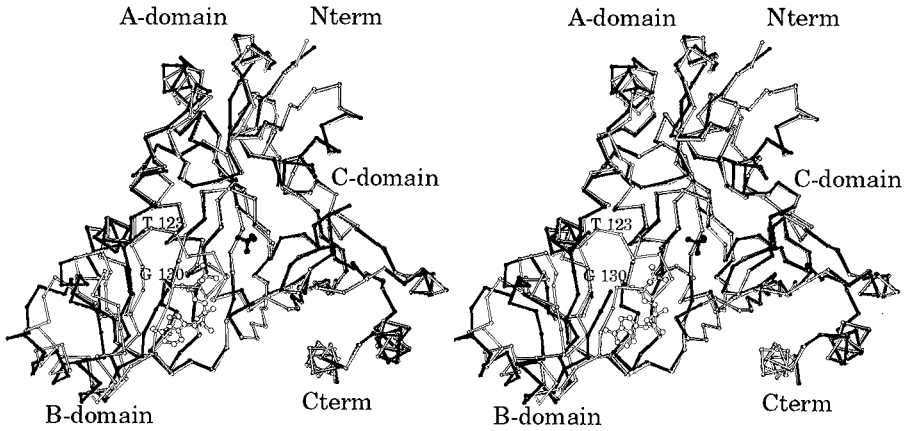

FIGURE 8: Superposition of the polypeptide chains for the native PurK and the PurK/MgADP complex. α-Carbon traces for the native enzyme and for the PurK/MgADP complex are displayed with solid and open bonds, respectively. The sulfate ion and the MgADP ligand are depicted in ball-and-stick representations.

containing Glu49 and Glu51 to move upon AIR binding, a signal that may be relayed directly to the sulfate (bicarbonate/carboxyphosphate) binding site via the Glu51−Arg242 interaction.

Postulated Mechanism. The conversion of an acid to an acyl phosphate is a common strategy employed in C−N ligases, many of which have been shown to adopt the newly recognized ATP grasp motif (*17*). ATP grasp enzymes all employ $MgATP^3$ but couple together a wide variety of donor and acceptor molecules. The observation that CPS, BC, and PurK all contain this molecular architecture points toward a common mechanism for both bicarbonate positioning and carboxyphosphate formation and utilization.

Carboxyphosphate is very unstable and has never been observed directly (*45*). In general the role of carboxyphosphate has been believed to be the generation of CO_2, which is attacked by an amine nucleophile (*46*). However, recent studies of Raushel and co-workers (*47*) on the bicarbonate-dependent ATPase reaction of CPS suggests that this is not the case, at least in the absence of amine cosubstrate (*47*). The recent structures of DDL and GTS with tight-binding inhibitors that become phosphorylated (*20*, *48*) suggest an alternative mechanism for the reaction of carboxyphosphate with amine. If the ATP grasp superfamily utilizes a common mechanism, then the amine attacks the carboxyl group of carboxyphosphate to form a tetrahedral intermediate, which then collapses to form product.

In addition, the structure of PurK resembles several members of the purine biosynthetic pathway including PurD (*22*) and, as inferred by its high degree of sequence similarity to PurK, PurT (*42*). By analogy with the carboxyphosphate intermediate proposed for PurK, the reaction mechanism of PurD is proposed to utilize a glycyl phosphate intermediate (*41*), while PurT is known to utilize a formyl phosphate intermediate. Recent studies on PurT detected the formyl phosphate intermediate by using a mutant in the B loop of the B domain (*49*).

To more fully address those structural features responsible for AIR binding to PurK and the role of the metal ions and to compare and contrast the active-site geometry of PurK with other members of the ATP grasp superfamily, cocrystallization trials with AMPPCP and AIR are presently in progress.

ACKNOWLEDGMENT

We thank Dr. W. W. Cleland for critically reading the manuscript.

REFERENCES

1. Buchanan, J. M., and Hartman, S. C. (1959) *Adv. Enzymol. Relat. Areas Mol. Biol. 39*, 91−183.
2. Firestine, S. M., Poon, S.-W., Mueller, E. J., Stubbe, J., and Davisson, V. J. (1994) *Biochemistry 33*, 11927−11934.
3. Meyer, E., Leonard, N. J., Bhat, B., Stubbe, J., and Smith, J. M. (1992) *Biochemistry 31*, 5022−5032.
4. Mueller, E. J., Meyer, E., Rudolph, J., Davisson, V. J., and Stubbe, J. (1994) *Biochemistry 33*, 2269−2278.
5. Meyer, E., Kappock, T. J., Osuji, C., and Stubbe, J. (1999) *Biochemistry 38*, 3012−3018.
6. Mathews, I. I., Kappock, T. J., Stubbe, J., and Ealick, S. E. (1999) *Structure* (in press).
7. Polakis, S. E., Guchhait, R. B., Zwergel, E. E., Lane, M. D., and Cooper, T. G. (1974) *J. Biol. Chem. 249*, 6657−6667.
8. Climent, I., and Rubio, V. (1986) *Arch. Biochem. Biophys. 251*, 465−470.
9. Ogita, T., and Knowles, J. R. (1988) *Biochemistry 27*, 8028−8033.
10. Anderson, P. M., and Meister, A. (1965) *Biochemistry 4*, 2803−2809.
11. Raushel, F. R., and Villafranca, J. V. (1979) *Biochemistry 18*, 3424−3429.
12. Raushel, F. M., and Villafranca, J. V. (1980) *Biochemistry 19*, 3170−3174.
13. Waldrop, G. L., Rayment, I., and Holden, H. M. (1994) *Biochemistry 33*, 10249−10256.
14. Thoden, J. B., Holden, H. M., Wesenberg, G., Raushel, F. M., and Rayment, I. (1997) *Biochemistry 36*, 6305−6316.
15. Thoden, J. B., Raushel, F. M., Benning, M. M., Rayment, I., and Holden, H. M. (1999) *Acta Crystallogr. D 55*, 8−24.
16. Thoden, J. B., Wesenberg, G., Raushel, F. M., and Holden, H. M. (1999) *Biochemistry 38*, 2347−2357.
17. Galperin, M. Y., and Koonin, E. V. (1997) *Protein Sci. 6*, 2639−2643.
18. Wolodko, W. T., Fraser, M. E., James, M. N. G., and Bridger, W. A. (1994) *J. Biol. Chem. 269*, 10883−10890.
19. Herzberg, O., Chen, C. C., Kapadia, G., McGuire, M., Carroll, L. J., Noh, S. J., and Dunaway-Mariano, D. (1996) *Proc. Natl. Acad. Sci. U.S.A. 93*, 2652−2657.
20. Fan, C., Moews, P. C., Walsh, C. T., and Knox, J. R. (1994) *Science 266*, 439−443.
21. Yamaguchi, H., Kato, H., Hata, Y., Nishioka, T., Kimura, A., Oda, J., and Katsube, Y. (1993) *J. Mol. Biol. 229*, 1083−1100.
22. Wang, W., Kappock, T. J., Stubbe, J., and Ealick, S. E. (1998) *Biochemistry 37*, 15647−15662.

23. Almassy, R. J., Janson, C. A., Kan, C. C., and Hostomska, Z. (1992) *Proc. Natl. Acad. Sci. U.S.A. 89*, 6114−6118.
24. Yount, R. G., Babcock, D., Ballantyne, W., and Ojala, D. (1971) *Biochemistry 10*, 2484−2489.
25. Kabsch, W. (1988) *J. Appl. Crystallogr. 21*, 67−71.
26. Kabsch, W. (1988) *J. Appl. Crystallogr. 21*, 916−924.
27. Terwilliger, T. C., and Eisenberg, D. (1983) *Acta Crystallogr. A 39*, 813−817.
28. Rossmann, M. G. (1960) *Acta Crystallogr. 13*, 221−226.
29. Wang, B. C. (1985) *Methods Enzymol. 115*, 90−112.
30. Tiedeman, A. A., Keyhani, J., Kamholz, J., Daum, H. A., 3d, Gots, J. S., and Smith, J. M. (1989) *J. Bacteriol. 171*, 205−212.
31. Watanabe, W., Sampei, G., Aiba, A., and Mizobuchi, K. (1989) *J. Bacteriol. 171*, 198−204.
32. Tronrud, D. E., Ten Eyck, L. F., and Matthews, B. W. (1987) *Acta Crystallogr. A 43*, 489−501.
33. Navaza, J. (1994) *Acta Crystallogr. A 50*, 157−163.
34. Bricogne, G. (1976) *Acta Crystallogr. A 32*, 832−847.
35. Kabsch, W., and Sander, C. (1983) *Biopolymers 22*, 832−847.
36. Holm, L., and Sander, C. (1996) *Science 273*, 595−602.
37. Krahn, J. M., Kim, J. H., Burns, M. R., Parry, R. J., Zalkin, H., and Smith, J. L. (1997) *Biochemistry 36*, 11061−11068.
38. Hara, T., Kato, H., Katsube, Y., and Oda, J. I. (1996) *Biochemistry 35*, 11967−11974.
39. Esser, L., Wang, C. R., Hosaka, M., Smagula, C. S., Sudhof, T. C., and Deisenhofer, J. (1998) *EMBO J. 17*, 977−984.
40. Lee, B., and Richards, F. M. (1971) *J. Mol. Biol. 55*, 379−400.
41. Cheng, Y.-S., Rudolph, J., Stern, M., Stubbe, J., Flannigan, K. A., and Smith, J. M. (1990) *Biochemistry 29*, 218−227.
42. Marolewski, A., Smith, J. M., and Benkovic, S. J. (1994) *Biochemistry 33*, 2531−2537.
43. Thoden, J. B., Miran, S. G., Phillips, J. C., Howard, A. J., Raushel, F. M., and Holden, H. M. (1998) *Biochemistry 37*, 8825−8831.
44. Polekhina, G., Board, P. G., Gali, R. R., Rossjohn, J., and Parker, M. W. (1999) *EMBO J. 18*, 3204−3213.
45. Sauers, C. K., Jencks, W. P., and Groh, S. (1975) *J. Am. Chem. Soc. 97*, 5546−5553.
46. Knowles, J. R. (1989) *Annu. Rev. Biochem. 58*, 195−221.
47. Gibson, G. E., Mullins, L. S., and Raushel, F. M. (1998) *Bioorg. Chem. 26*, 255−268.
48. Hiratake, J., Kato, H., and Oda, J. (1994) *J. Am. Chem. Soc. 116*, 12059−12060.
49. Marolewski, A. E., Mattia, K. M., Warren, M. S., and Benkovic, S. J. (1997) *Biochemistry 36*, 6709−6716.
50. Nicholls, A., Sharp, K., and Honig, B. (1991) *Proteins: Struct., Funct. Genet. 11*, 281−296.
51. Kraulis, P. J. (1991) *J. Appl. Crystallogr. 24*, 946−950.
52. Merritt, E. A., and Bacon, D. J. (1997) *Methods Enzymol. 277*, 505−524.

BI991618S